Geoscience Frontiers 8 (2017) 457–465

HOSTED BY

Contents lists available at ScienceDirect

China University of Geosciences (Beijing)

Geoscience Frontiers

journal homepage: www.elsevier.com/locate/gsf

Research paper

Lunar surface mineralogy using hyperspectral data: Implications for primordial crust in the Earth–Moon system

V. Sivakumar [a,b,*], R. Neelakantan [b,c], M. Santosh [d,e,f]

[a] Centre for Development of Advanced Computing (C-DAC), CDAC Innovation Park, Pune, 411008, India
[b] Department of Geology, Periyar University, Salem, 636011, India
[c] Department of Industries and Earth Sciences, Tamil University, Tanjore, 613010, India
[d] Centre for Tectonics, Resources and Exploration, Department of Earth Sciences, University of Adelaide, SA, 5005, Australia
[e] School of Earth Sciences and Resources, China University of Geosciences Beijing, 29 Xueyuan Road, Beijing, 100083, China
[f] Faculty of Science, Kochi University, Kochi, 780-8520, Japan

ARTICLE INFO

Article history:
Received 15 December 2015
Received in revised form
15 March 2016
Accepted 23 March 2016
Available online 12 April 2016
Handling Editor: E. Shaji

Keywords:
Moon Mineralogy Mapper
Lunar Magma Ocean
Primordial crust
Magmatic differentiation
Chandrayaan-1

ABSTRACT

Mineralogy of the Lunar surface provides important clues for understanding the composition and evolution of the primordial crust in the Earth–Moon system. The primary rock forming minerals on the Moon such as pyroxene, olivine and plagioclase are potential tools to evaluate the Lunar Magma Ocean (LMO) hypothesis. Here we use the data from Moon Mineralogy Mapper (M^3) onboard the Chandrayaan-1 project of India, which provides Visible/Near Infra Red (NIR) spectral data (hyperspectral data) of the Lunar surface to gain insights on the surface mineralogy. Band shaping and spectral profiling methods are used for identifying minerals in five sites: the Moscoviense basin, Orientale basin, Apollo basin, Wegener crater-highland, and Hertzsprung basin. The common presence of plagioclase in these sites is in conformity with the anorthositic composition of the Lunar crust. Pyroxenes, olivine and Fe-Mg-spinel from the sample sites indicate the presence of gabbroic and basaltic components. The compositional difference in pyroxenes suggests magmatic differentiation on the Lunar surface. Olivine contains OH/H_2O band, indicating hydrous phase in the primordial magmas.

1. Introduction

Mineral mapping of the Lunar surface provides insights into the composition and evolution of the crust and also provides important information on the primordial crust in the Earth–Moon system. The Lunar Magma Ocean (LMO) hypothesis envisages that the Moon was completely molten to hundreds of kilometers depth immediately after its accretion (e.g., Wood et al., 1970). The major minerals crystallising from LMO would include olivine, pyroxenes and plagioclase (e.g., Taylor and Bence, 1975; Warren, 1985; Papike et al., 1997). Therefore Lunar mineralogy provides important clues for the evolution of the planet's crust from the earliest LMO cumulates, through the plagioclase flotation crust to later intrusive and extrusive process. Furthermore, considering the similarities in the Hadean history of Earth and Moon, characterising the Lunar crust would also provide information on the primordial crust of the Earth, which has been subsequently destroyed through plate tectonic processes (e.g., Kawai et al., 2009; Maruyama et al., 2013).

The Moon has been explored using several unmanned and manned missions between 1960's and 1990's. These explorations have yielded valuable information on the physical and chemical properties of the Moon. The scientific explorations through post-Apollo orbital satellites like Galileo, Clementine, Lunar Prospector, and the discovery of Lunar meteorites have significantly added to our understanding of the evolution of this planet.

Advancements in orbital satellite technology have allowed the evaluation of surface lithology of the Moon through mineralogical mapping using high spectral and spatial resolution data (e.g. SELENE Spectral Profiler, Multi-band Imager and Moon Mineralogy Mapper (M^3)). The M^3 on-board Chandrayaan-1, the Indian Space Research Organisation's (ISRO) first mission to the Moon (Goswami and Annadurai, 2009), provides information about the Lunar surface mineralogy. This study reports an analysis of the Lunar surface

* Corresponding author. Centre for Development of Advanced Computing (C-DAC), CDAC Innovation Park, Pune, 411008, India.
E-mail address: v.sivakumars@gmail.com (V. Sivakumar).
Peer-review under responsibility of China University of Geosciences (Beijing).

http://dx.doi.org/10.1016/j.gsf.2016.03.005

mineralogy using M^3 data with a view to understand the composition of the Lunar crust.

2. Regional setting and study areas

The study areas are shown on the crustal thickness map of Moon in Fig. 1. To understand the Moon's crustal composition both vertically and laterally, representative areas were selected in different regions on the planet's surface based on published literature and crustal thickness map (Gravity Recovery and Interior Laboratory, GRAIL). The crustal thickness map offers information on the crustal density of the Moon, which can be correlated with rock composition (Wieczorek et al., 2013). The Lunar composition varies with crustal thickness and plagioclase-rich domains of anorthositic crust are found in regions of higher crustal thickens as compared to the thinner mafic crust of possibly basaltic/gabbroic composition (Cahill et al., 2009). Thus, crustal thickness map is one of the key bases for sample site selection.

2.1. Apollo basin (SPA) (sample site 1)

Apollo basin is located inside the South Pole-Aitken basin (SPA) (Fig. 1), which is considered to reflect the lower crustal composition of the Moon. The SPA basin is one of the oldest and largest recognised impact structures in the Solar system, and the basin is about 2600 km in diameter, with an average depth of about 12 km (e.g., Spudis et al., 1994). The basin formed after the solidification of Lunar crust. Apollo basin is a large (538 km), double-ringed impact crater on the far side, at latitude 36°S and longitude 152°W. The basin represents a concentric, double-ring impact structure, transitional in size between smaller simple bowl-shaped and complex central peak or peak-ring craters and larger impact basins like Orientale basin (Wilhelms et al., 1979). The basin formed at ca. 3.85 Ga (e.g., Craddock and Howard, 2000), post-dating the formation of SPA and lies in the north eastern periphery of SPA basin.

2.2. Orientale basin (sample site 2)

Orientale basin is located on the western limb of the Moon highland terrain and centered at 19°S, 95°W (Fig. 1). This basin is the youngest and most well-preserved large multi ring basin on the Moon and sparsely filled by mare basalt (e.g., Wilhelms, 1987). The Orientale is a large impact structure basin and displays at least four concentric rings (multi-ring basin) (e.g., Wilhelms, 1987; Spudis, 1993). This basin has been explored by many workers (e.g., Whitten et al., 2011; Cheek et al., 2013; Donaldson Hanna et al., 2014; Arivazhagan, 2015) who identified clinopyroxene, orthopyroxene, plagioclase and olivine. The rocks in this location can therefore be considered as products of differentiation of the Lunar Magma Ocean.

2.3. Moscoviense basin (sample site 3)

The Moscoviense basin is centered at 27°N, 146°E and located in the Lunar far side highland terrane (Fig. 1) from where the thinnest crust has been reported among all the other basins measured on the Moon (Wieczorek et al., 2013). Mare Moscoviense basin covers an area of 35,000 km^2 (Gillis, 1998) and is assumed to be the result of a major impact during 3.85–3.92 Ga (Wilhelms, 1987). The basin experienced subsequent mare volcanism during 3.2–3.8 Ga (e.g., Kramer et al., 2008), with final basalt flows between 2.5–2.6 Ga (e.g., Haruyama et al., 2009). The unique geologic setting of Moscoviense basin may provide information about Lunar lower crust. This basin has also been explored several workers (e.g., Bhattacharya et al., 2011; Pieters et al., 2011) who identified five major compositional units such as feldspathic matrix, Mg-rich spinel, highland basin soils, ancient mature mare, highland

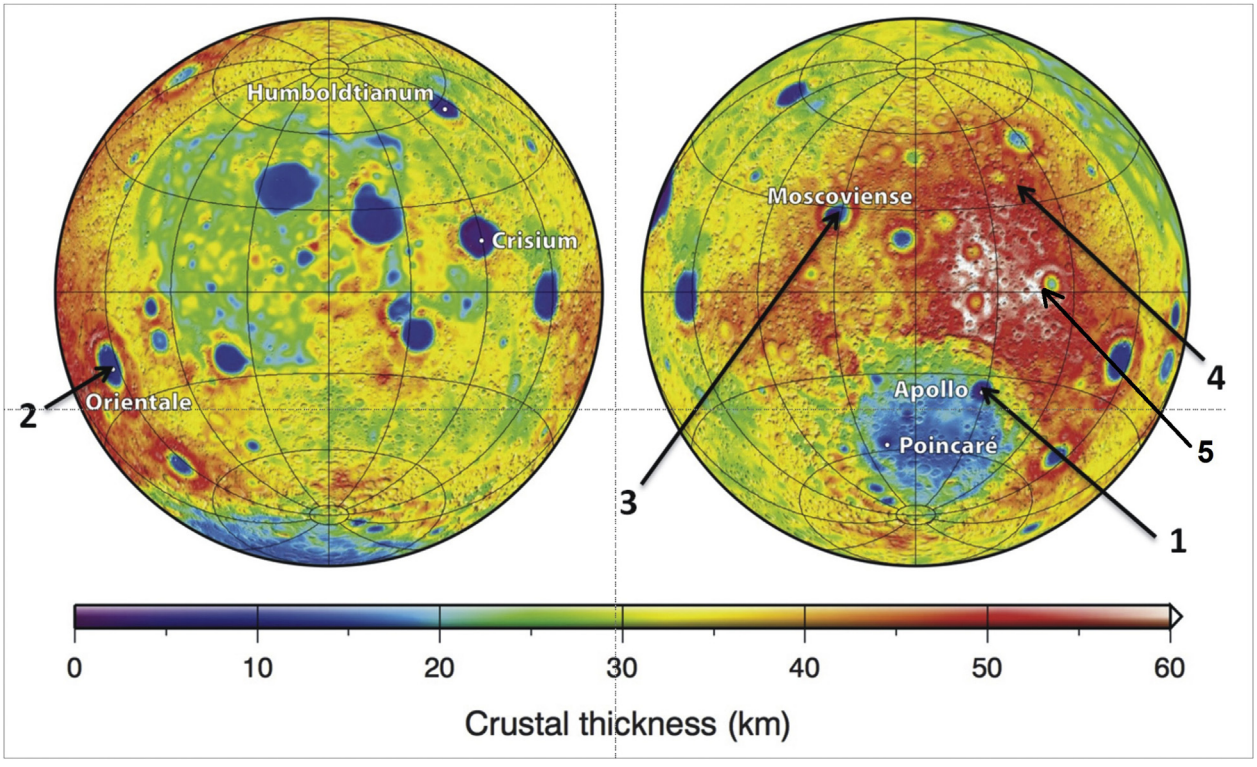

Figure 1. Colour coded crustal thickness map of the Moon derived from GRAIL (Wieczorek et al., 2013). Black colour arrows indicate the sample site locations. Numbers 1–4 show sample site number: 1 – Apollo basin; 2 – Orientale basin; 3 – Moscoviense basin; 4 – Wegener crater (highland); 5 – Hertzsprung basin.

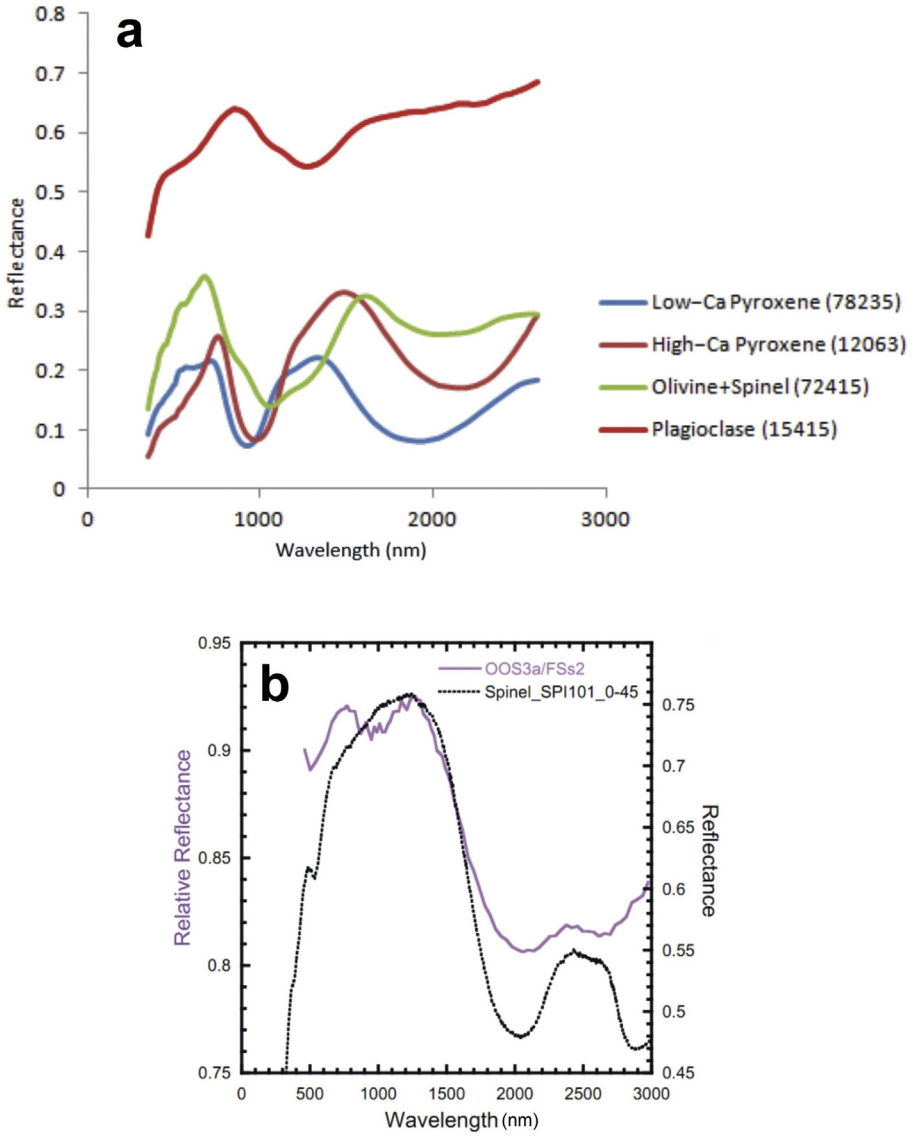

Figure 2. (a) RELAB reflectance spectra of olivine, plagioclase, low and high Ca pyroxenes. (b) Mg-spinel spectra (Reflectance spectrum of spinel-rich area OOS3a relative to featureless FS soil compared with a laboratory spectrum of Mg-rich spinel (Cloutis et al., 2004)). Image source: Pieters et al. (2010).

contaminated mare, buried unit with abundant low-Ca pyroxene (LCP), and youngest mare unit.

2.4. Wegener crater-highlands (sample site 4)

Wegener crater area is located in the highland region (far side) of the Moon (Fig. 1). It is topographically rugged terrain due to large number (high frequency) of impact craters. The crustal thickness is high in the study area suggesting exposure of fractionated products from the LMO. The study area is located in the higher latitude region and extends from approximately 113°–119°W and 42°–49°N (Fig. 1). The general elevation ranges varies from −1000 m to 3000 m approximately (elevation value are collected form Lunar Reconnaissance Orbiter Camera (LROC) data). The sampling sites are from ~100 m to 3000 m elevation range. Geologically, the area is considered to range in age from older than 3.92 to 3.2 Ga (Wilhelms, 1984).

2.5. Hertzsprung basin (sample site 5)

The Hertzsprung basin is located (2°N, 128°W) in the area of the topographically highest region of the Moon (e.g., Wilhelms, 1987; Spudis, 1993) (Fig. 1). The basin is a relatively well-preserved impact basin of Nectarian age on the far side of the Moon (e.g., Wilhelms, 1987). The basin is 570 km wide, with an average depth of about 4.5 km and rim height of 1.06 km (e.g., Spudis, 1993; Spudis and Adkins, 1996). The crustal thickness in this basin region is roughly 60 km (Fig. 1). The Hertzsprung basin is an intermediate-sized basin and might have excavated material from depths, hence providing information about compositions and lithologies occurring at middle levels of the Lunar crust (e.g., Stockstill and Spudis, 1998). This basin also represents the uppermost section of the lunar crust. Spectral samples were collected from the western side of the basin (Fig. 7).

3. Data acquisition

The M^3 hyperspectral data is used for mapping and analysing mineral compositions from different sample sites. The M^3 sensor was a guest instrument from NASA on the Chandrayaan-1 (Goswami and Annadurai, 2009). The sensor records the reflected radiance from the Moon's surface in pushbroom mode between 0.46 and 2.97 μm in 85 contiguous spectral bands, between

Table 1
A summary of the band shape algorithm techniques (modified after Borst et al., 2012; Sivakumar and Neelakantan, 2015).

Name of band shape (ratio) algorithms	Algorithms	Colour	Minerals			
			Olivine	Low-Ca pyroxene	High-Ca pyroxene	Anorthosite
Band strength	1008/750 nm	Blue	Low	Medium + Low	Highest	Highest
Band curvature	750/910 + 1008/910 nm	Red	Medium	High + Highest	Lowest	Medium
Band tilt	910/1008 nm	Green	Low	High + Low	Medium	Lowest
Olivine/Pyroxene	2018/1008 nm	Black/White	High	Lowest + Low	Low	low

20–40 nm spectral sampling and 140 m/pixel across the 40 km field of view (Pieters et al., 2009). Photometrically and thermally corrected Level-2 data are used for this study. The LROC data (Robinson et al., 2010) and GRAIL spacecraft derived results are used for understanding the topography of the sample sites and Lunar crustal thickness (Wieczorek et al., 2013) (Fig. 1), respectively. The coverage of the M^3 level-2 data for the sample sites are restricted to the single optical period, as there is no significant absorption band shift in different optical period images due to sensor thermal effect (Whitten and Head, 2015). The RELAB lab spectra (Fig. 2a), Mg-Spinel (Fig. 2b) spectrum (Cloutis et al., 2004) and published mineral spectra are used for comparison and identification of minerals.

4. Methodology

4.1. Mineral mapping

The Lunar minerals are recognised in visible to near-infrared reflectance spectra (remote sensing) by distinct absorption bands. The absorption is a result of photon interaction with the crystal fields (e.g., Burns, 1993). The mineral composition, crystal arrangement, grain size, space weathering, regolith cover, etc control the absorption graph shape, strength, and wavelength position. Therefore, distinguishing and quantifying composition of the minerals are challenging. To minimise the error in mineral identifications due to effect of space weathering and regolith cover, the data analysed are from the brighter (fresh) exposures on the M^3 imagery. The analysis of minerals is limited to 750–1500 nm, 1800–2300 nm wavelength regions particularly since the major minerals such as olivine, pyroxenes and plagioclase are present in these spectral regions. The ENVI image processing software is used for clipping of image for the study area, executing band/spectral mathematical expressions to perform mathematical operations on the M^3 data, creating RGB composite, mapping the minerals, spectral sample collection, spectral profile manipulation/visualisation, continuum removing and comparison with lab and published spectra.

4.1.1. Band shape algorithms

The band shape algorithms such as band strength (bs), band curvature (bc), band tilt (bt) and band ratio (br) are employed at crucial wavelengths to delineate the abundance of minerals such as olivine, low-Ca pyroxene, high-Ca pyroxene and plagioclase on the Lunar surface. The bs, bc, bt and br at crucial wavelengths (approximate) are calculated, with ratios between 1009/750 nm, 750/910 nm + 1009/910 nm, 910/1009 nm and 2018/1009 nm respectively (Table 1). The above approach is appropriate to distinguish specific minerals in a false colour composite map. These techniques are systematically used for Clementine UV/VIS and NIR data by Borst et al. (2012), has also been expanded to the M^3 data by Sivakumar and Neelakantan (2015) to discriminate the specific minerals. This method also facilitates in grouping similar pixels (end members) and aids to model the spectral profile effectively.

4.1.2. Spectral profile analysis

The ENVI image processing software is used for deriving spectral profiles and continuum removal of sampled spectra. More than 100 samples (3×3 pixels average) are collected from five study sectors, although only representative (19 samples) spectral samples have been used for analysis. Similar or overlapping samples are not considered and only representative samples are used for final analysis. Automatic straight-line approximations continuum-removal method is used for removing background continuum (e.g., Clark and Roush, 1984; Clark et al., 1987) to filter the residual absorption band shapes. These sampled spectral profiles are exported to ASCII standard format to perform further analysis and create better spectral graphs. The OriginPro v8.0 software is used to derive parameters such as band shape, band-depth and band-centre for understanding of absorption characteristics.

5. Results

The major minerals mapped in Apollo (site 1), Orientale (site 2), Moscoviense (site 3), Wegener crater-highland (site 4) and Hertzsprung (site 5) image spectral sample sites are discussed in the following subsections. Table 2 shows minerals identified and their locations. Major minerals such as pyroxenes, olivine and plagioclase are identified in the five different sample sites based on absorption characteristics and lab and published Lunar mineral spectra. Their occurrence, origin, and probable source are discussed in subsequent sections.

5.1. Apollo basin (SPA) (sample site 1)

Fig. 3a shows the ratio of 2018/1008 nm and the results show high intensity values (brighter appearances) on the image, suggesting possible olivine-rich mineral assemblages (e.g., Borst et al., 2012). Fig. 3b shows RGB composite of bs, bc and bt. The bs values are high (appearing in blue colour), which probably indicates mafic poor/weathered rocks. Generally, soils derived from space weathering show high bs values (e.g., Tompkins et al., 1997). The bc indicates presence of LCP (pyroxene with high Fe/Mg) in the Lunar

Table 2
Identified minerals and their locations (image spectral sample site).

Minerals	Location
Low Ca-pyroxene	Orientale basin, Apollo basin, Moscoviense basin, Wegener Crater (highland) and Hertzsprung basin
High Ca-pyroxene	Moscoviense basin, Apollo basin and Orientale basin
Olivine	Moscoviense basin, Orientale basin and Apollo basin
Plagioclase	Orientale basin, Wegener Crater (highland) and Hertzsprung basin
Fe-Mg-spinel lithology	Moscoviense basin, Orientale basin, Apollo basin, Wegener Crater (highland) and Hertzsprung basin

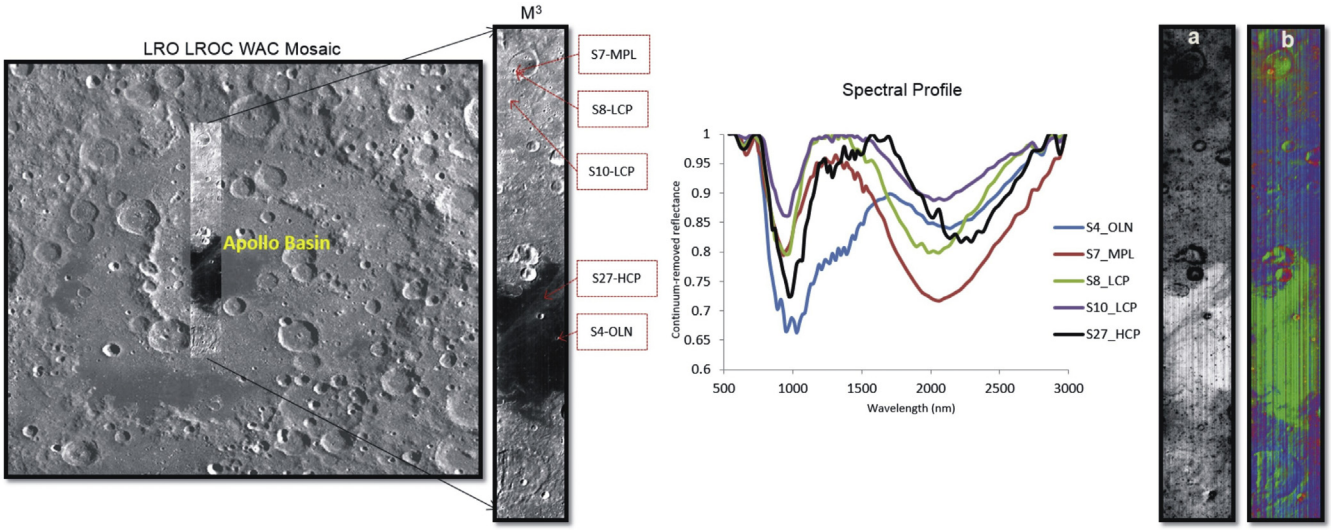

Figure 3. Continuum removed reflectance spectra (middle panel). Sample locations are highlighted on M^3 image. M^3 coverage is shown on LRO LROC WAC image (left panel). (a) Grayscale image (right panel) shows the ratio of 2018 nm/1008 nm; (b) RGB composite (right panel) of bs, bc and bt.

surface, which appears as red-pink colour in the RGB composite image. Higher band tilt value (appearing green-yellow colour) indicates mafic rocks with olivine such as komatiites or olivine gabbros.

Fig. 3 shows the continuum removed reflectance spectra of Apollo basin samples (S4_OLN, S8_LCP, S10_LCP, S7-MPL and S27_HCP). Sample No. S4_OLN shows strong absorption band near 1000 nm and there is no significant absorption near 2000 nm, indicating the presence of olivine (e.g., Isaacson et al., 2011). Sample-S8_LCP & S10_LCP show diagnostic absorption bands near 1000 nm and 2000 nm wavelength regions due to Mg^{2+}/Fe^{2+} contribution in the M1 and M2 crystallographic sites (e.g., Adams, 1974). These specific absorption indicate the presences of LCP. The LCP dominant rocks are found on the outer ring of the basin. HCP mineral is identified (Sample No. S27-HCP) based on M2 crystallographic site shift towards longer wavelength (absorption beyond 900 and 2300 nm) as a result of Ca^{2+} contribution. Sample-S7_MPL shows relatively weak absorption near 1000 nm and strong absorption near 2000 nm, suggesting the presence of Fe-Mg-spinel (e.g., Cloutis et al., 2004; Jackson et al., 2014; Pieters et al., 2014; Pathak et al., 2015).

5.2. Orientale basin (sample site 2)

The possible olivine-rich areas in this basin were delineated through ratio of 2018/1008 nm. The high ratio indicates the presence of olivine or mafic intrusive rocks (e.g., Borst et al., 2012) (Fig. 4a). Fig. 4b (RGB composite) shows high bs values (appearing in blue colour), which probably indicate plagioclase/mafic poor/weathered rock. The bc indicates presence of LCP/mafic and rich

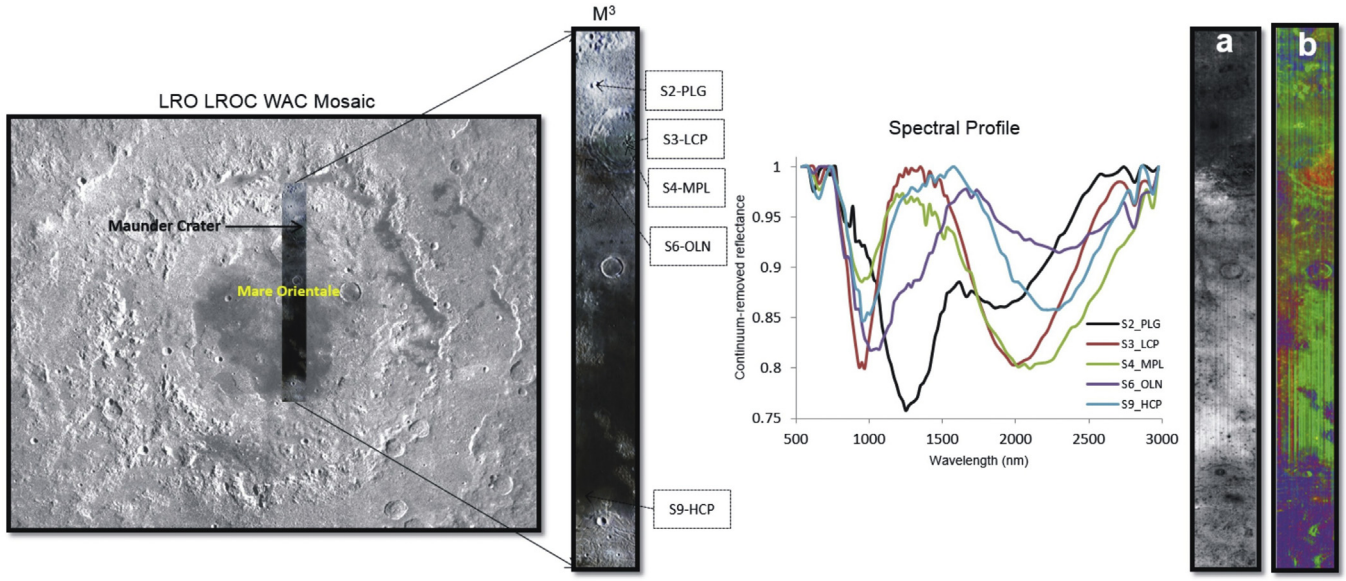

Figure 4. Continuum removed reflectance spectra (middle panel). Sample locations are highlighted on M^3 image. M^3 coverage is shown on LRO LROC WAC image (left panel). (a) Grayscale image (right panel) shows the ratio of 2018 nm/1008 nm; (b) RGB composite (right panel) of bs, bc and bt.

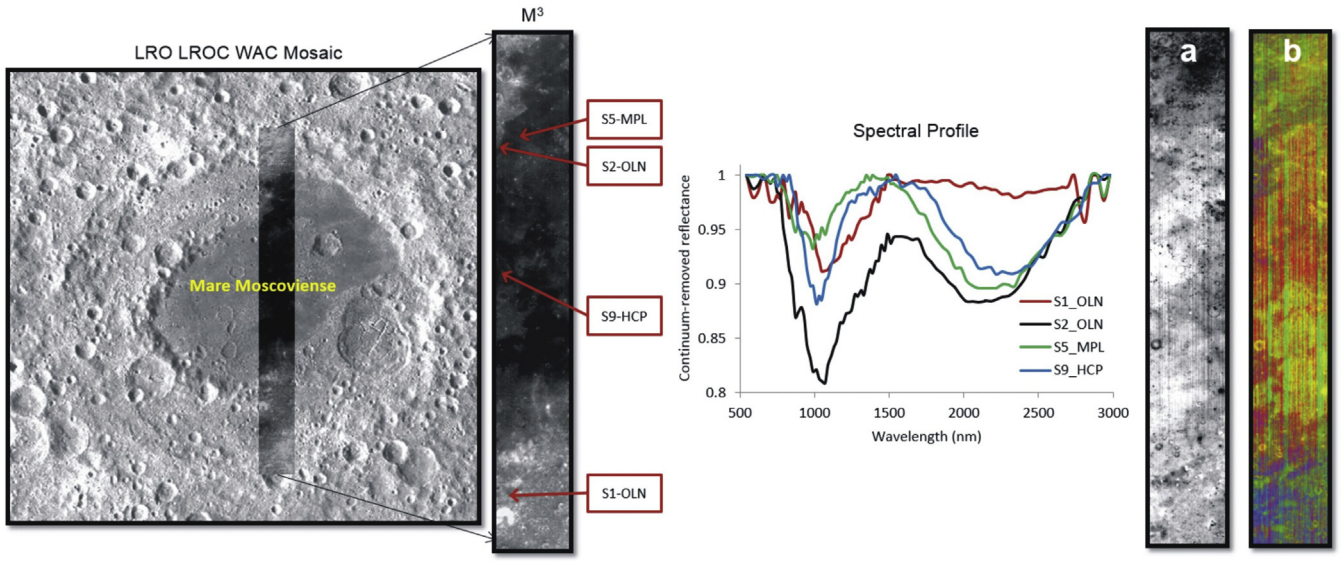

Figure 5. Continuum removed reflectance spectra (middle panel). Sample locations are highlighted on M^3 image. M^3 coverage is shown on LRO LROC WAC image (left panel). (a) Grayscale image (right panel) shows the ratio of 2018 nm/1008 nm; (b) RGB composite (right panel) of bs, bc and bt.

lithology, which appears in red-pink colour in RGB composite. Higher band tilt value (appearing in green-yellow colour) indicates olivine-bearing lithology.

Fig. 4 shows the continuum removed reflectance spectra of minerals such as olivine (Sample No. S6-OLN), LCP (Sample No. S3-LCP), HCP (Sample No. S9-HCP), plagioclase (Sample No. S2-PLG) and Fe-Mg-spinel (Sample No. S4-MPL). Olivine shows strong absorption band near 1000 nm (e.g., Isaacson et al., 2011). LCP shows absorption bands near 1000 nm and 2000 nm. HCP shows absorption band shift towards longer wavelength due to Ca^{2+} contribution. Plagioclase shows absorption band near 1250 nm due to Fe^{2+} (e.g., Conel and Nash, 1970; Adams and Goullaud, 1978). Plagioclase spectrum (S2-PLG) also shows 2000 nm absorption suggesting the possible presence of pyroxenes (e.g., Chauhan et al., 2012). Fe-Mg-spinel shows typical strong absorption near 2000 nm and weaker band 1000 nm (e.g., Cloutis et al., 2004; Jackson et al., 2014; Pieters et al., 2014; Pathak et al., 2015).

5.3. Moscoviense basin (sample site 3)

Results shown in Fig. 5a suggest olivine/mafic rich intrusive rock (e.g., Borst et al., 2012), with high band ratio. Mafic intrusive/lower crust material appears bright in grayscale image (e.g., Borst et al., 2012). Fig. 5b shows RGB composite of band ratios (bs, bc and bt). The bs values are high (appearing in blue colour), which probably indicates mafic poor/weathered rock. The high bc indicates presence of LCP which appears in red-pink colour in RGB composite. Higher band tilt value shows green-yellow colour, suggesting olivine-rich lithology.

Fig. 5 shows the continuum removed spectra. Sample No. S1-OLN shows olivine with OH/H_2O band (absorption near 2800 nm) (e.g., Clark, 2009; Pieters et al., 2009; Cheek et al., 2011; Bhattacharya et al., 2015). Sometimes, the strength and position of the absorption spectra near 2800 nm region may be due to illumination and thermal conditions. Recent studies confirm that the strength of the OH/H_2O feature does not vary in different date M^3 images and under sun illumination condition of spectra (e.g., Cheek et al., 2011; Chauhan and Kaur, 2014) with no significant shift in absorption band (Whitten and Head, 2015). Olivine rich area is located in the southern edge of the inner ring of the basin. An olivine rich spectrum shows strong absorption near 1000 nm (e.g., Isaacson et al., 2011). The spectra shows typical absorption bands near 2800 nm wavelength regions due to OH/H_2O content (e.g., Clark, 2009; Pieters et al., 2009; Bhattacharya et al., 2015). Sample No. S2-OLN shows absorption near 1000 nm, indicating olivine, although another week absorption near 2000 nm is also noted, which probably corresponds to chromite inclusions (e.g., Isaacson et al., 2011; Cheek and Pieters, 2014). Data from sample No. S5-MPL show Fe-Mg-spinel lithology (e.g., Cloutis et al., 2004; Jackson et al., 2014; Pieters et al., 2014; Pathak et al., 2015) and sample No. S9-HCP indicates presences of HCP.

5.4. Wegener crater-highlands (sample site 4)

Fig. 6a shows possible olivine (mafic) rich area, which is highlighted in high ratio (bright appearance) (e.g., Borst et al., 2012). Fig. 6b shows RGB composite of band ratios (bs, bc and bt). The blue colour shows high bs values which indicates anorthositic/weathered/mafic poor rocks. The bc indicates presence of LCP in the Lunar surface, which appears in red-pink colour in RGB composite. Higher band tilt value (appearing green-yellow colour) indicates mafic rich rocks.

Fig. 6 shows the continuum removed reflectance spectra of Wegener crater region. LCP rich areas are observed from the three different locations. LCP are identified based on absorption bands near 1000 nm and 2000 nm due to electronic transition in M1 and M2 crystallographic sites. Sample S3-LCP shows stronger absorption due to Fe^{2+} contribution. Sample S2-PLG shows strong absorption near 1250 nm and weak absorption near 2000 nm indicating that plagioclase with pyroxene lithology corresponding to anorthositic gabbro or gabbro (e.g., Chauhan et al., 2012). However, absorption spectrum is not even, may be due to space weathering/sun angle. Fe-Mg-spinel (Sample No. S5-MPL) shows a typical strong absorption near 2000 nm and weaker band 1000 nm (e.g., Cloutis et al., 2004; Jackson et al., 2014; Pieters et al., 2014; Pathak et al., 2015).

5.5. Hertzsprung basin (sample site 5)

The mafic compositions were demarcated based on the ratio of 2018/1008 nm. The high ratio (brighter appearance) indicates the presence of mafic rocks (e.g., Borst et al., 2012) (Fig. 7a). The RGB

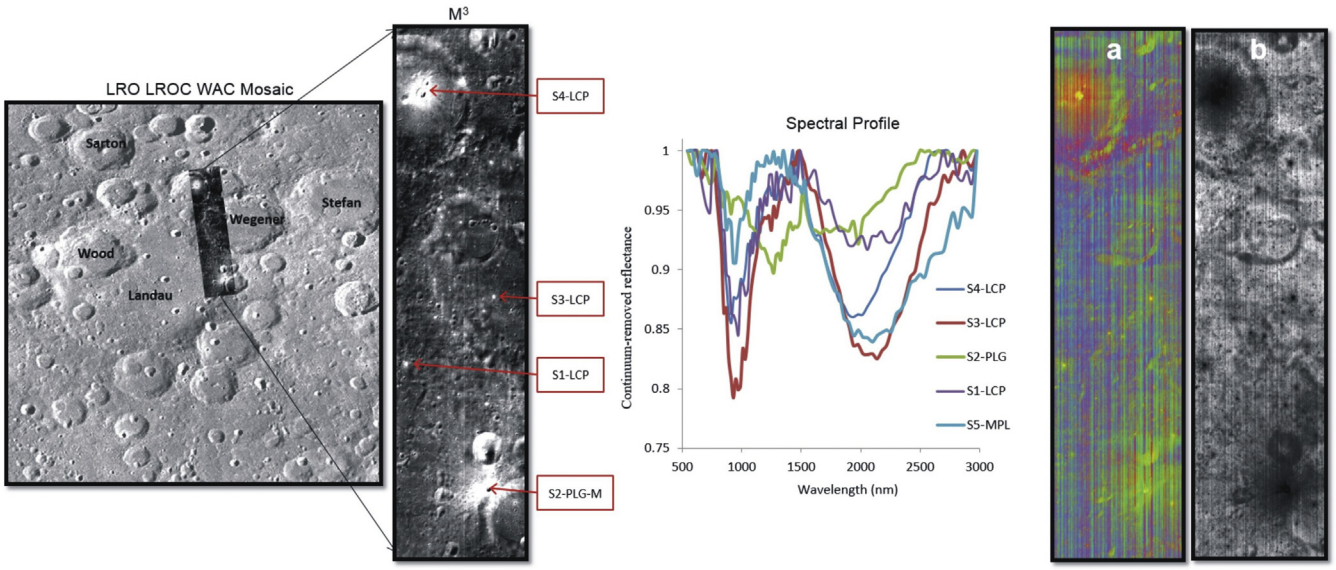

Figure 6. Continuum removed reflectance spectra (middle panel). Sample locations are highlighted on M^3 image. M^3 coverage is shown on LRO LROC WAC image (left panel). (a) Grayscale image (right panel) shows the ratio of 2018 nm/1008 nm; (b) RGB composite (right panel) of bs, bc and bt.

composite of bs, bc and bt indicates the possible plagioclase/mafic poor/weathered rock lithology (blue colour), LCP/mafic rich lithology (red-pink colour) and possible olivine-bearing lithology/high mafic (green-yellow colour), respectively.

The continuum removed reflectance spectra of plagioclase (Sample No. S1-PLG and S4-PLG), LCP (Sample No. S2-LCP and S6-LCP) and Fe-Mg-spinel (Sample No. S5-MPL) minerals are shown in the Fig. 7. LCP shows the spectral absorption near 1000 nm and 2000 nm wavelength region. Plagioclase shows absorption spectra near 1250 nm due to Fe^{2+} (e.g., Conel and Nash, 1970; Adams and Goullaud, 1978). Plagioclase spectrum also shows little amount of 2000 nm absorption suggesting the possible presence of pyroxenes lithology (e.g., Chauhan et al., 2012) (Fig. 7). Fe-Mg-spinel shows typical strong absorption near 2000 nm and weaker band 1000 nm (e.g., Cloutis et al., 2004; Jackson et al., 2014; Pieters et al., 2014; Pathak et al., 2015).

6. Discussion

Our study employed M^3 hyperspectral data for identifying primary minerals such as olivine, pyroxene and plagioclase from five regions on the Lunar surface. This confirms previous studies that M^3 data can be successfully employed for the identification and mapping of minerals on the Moon surface (e.g., Goswami and Annadurai, 2009; Pieters et al., 2009; Bhattacharya et al., 2011; Cheek et al., 2011; Isaacson et al., 2011; Pieters et al., 2011; Whitten et al., 2011; Chauhan et al., 2012; Cheek et al., 2013; Donaldson Hanna et al., 2014; Jackson et al., 2014; Pieters et al., 2014; Arivazhagan, 2015; Pathak et al., 2015; Sivakumar and Neelakantan, 2015). The olivine-bearing lithology is observed around large impact basin characterised by relatively thin crust, and might correspond to olivine-rich basalts or komatiites. The olivine samples from Mare Moscoviense (site 3) basin region contain OH/H_2O band near

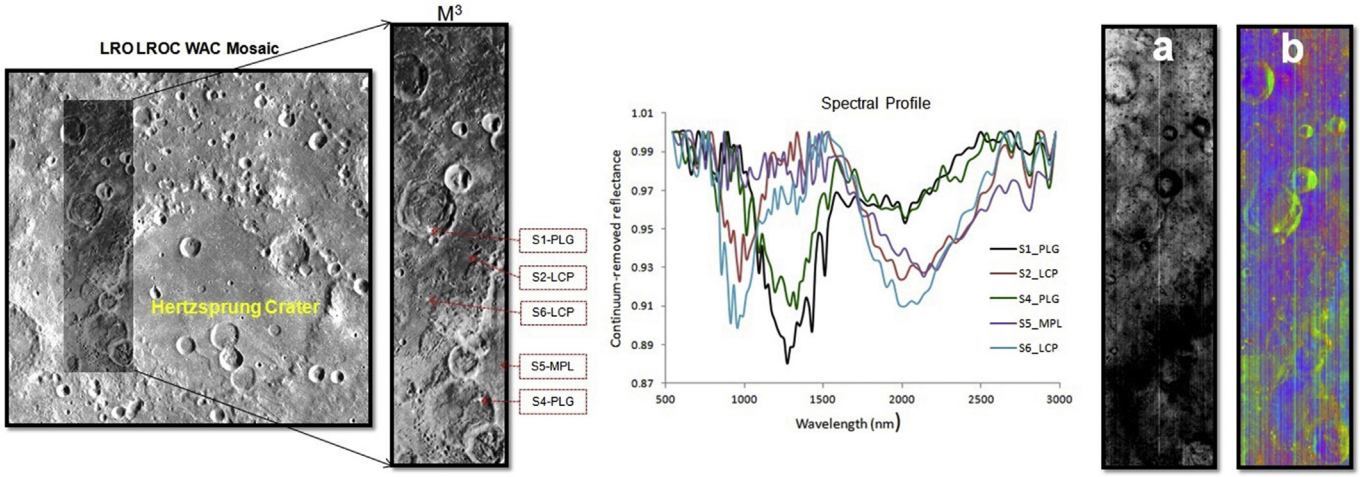

Figure 7. Continuum removed reflectance spectra (middle panel). Sample locations are highlighted on M^3 image. M^3 coverage is shown on LRO LROC WAC image (left panel). (a) Grayscale image (right panel) shows the ratio of 2018 nm/1008 nm; (b) RGB composite (right panel) of bs, bc and bt.

2800 nm indicating the presence of water in Lunar magma. This result is consistent with earlier studies (e.g., Klima et al., 2013; Sivakumar and Neelakantan, 2014; Bhattacharya et al., 2015). The presence of water molecules in Lunar magma was investigated through in-situ analysis and the results show that the Lunar Magma Ocean (LMO) which contributed to the formation of primordial crust was Hydrous. The water molecules were trapped within olivine crystals before eruption and there was no degassing after eruption (e.g., Hauri et al., 2011; Anand et al., 2014). The composition is broadly similar to primitive terrestrial mid-ocean ridge basalts and show that water molecules present in the parts of Lunar interior is comparable with Earth's upper mantle (e.g., Hauri et al., 2011). These findings have considerable implications for Lunar olivine and OH/H_2O signatures, which help in understanding the hydrous nature of Lunar lower crust. Pyroxene dominant-rocks (low Ca-pyroxenes and high Ca-pyroxenes) are identified near 900–1000 nm and 1900–2300 nm wavelength regions, as transition of Fe^{2+} in the M1 and M2 crystallographic sites of pyroxenes. Low Ca-pyroxene signature is predominantly found within Apollo basin (site 1), Orientale basin (site 2), Moscoviense basin (site 3), Wegener crater regions (site 4) (highland) and Hertzsprung basin (site 5). High Ca-pyroxene identified in the Orientale (site 2), Apollo basin (site 1) and Mare Moscoviense (site 3) basin regions. The occurrence of compositionally variable pyroxenes are analogous to anorthosite-gabbro complexes on the Earth, and suggest differentiation from primary basaltic magmas.

The presence of plagioclase is identified in Orientale (site 2), Wegener (site 4) and Hertzsprung basin (site 5) regions based on diagnostic plagioclase absorption band near 1250 nm in the M^3 spectra (e.g., Conel and Nash, 1970; Adams and Goullaud, 1978). Site 4 sample shows irregular spectral signature, probably indicating that the region was affected by space weathering (e.g., Tompkins et al., 1997). The presence of plagioclase is consistent with anorthositic crust, and also supports the LMO hypothesis (e.g., Cheek et al., 2013; Donaldson Hanna et al., 2014). With the onset of magmatic differentiation as magma cools, denser minerals like olivine and pyroxene sink and lighter plagioclase-rich material float to form the upper crust. The incompatible KREEP rich layer settled at the bottom of the plagioclase-rich cumulates and over the mafic-rich mantle (Hiesinger and Head, 2006). Thus, the identification and mapping of plagioclase-rich material on lunar surface provides key information for Lunar crustal evolution. The unusual spectral signatures observed from all the sectors analysed in this study is the weaker absorption band near 1000 nm and stronger absorption band near 2000 nm. This signature indicates the presences of probable Fe-Mg-spinel-bearing lithology on the Lunar surface. It has been suggested that the Fe-Mg-spinel lithology might form part of the extruded lower crustal material, which is exposed through major impacts or brought up by mafic intrusions (e.g., Pieters et al., 2014). Chromite-veined anorthosites are common in the Earth's crust and considering that the Lunar crust is dominantly composed of anorthosite, it is reasonable to envisage the presence of spinels. In summary, the mineralogical characterisation using hyperspectral data confirm that the major rock forming minerals on the Lunar surface are olivine, pyroxene and plagioclase, with additional presence of spinels. This is conformity with the lithological constitution of the Moon crust dominated by anorthosites, and subordinate KREEP basalts, komatiites and gabbros (e.g., Maruyama et al., 2013; Elrado et al., 2015). The mineralogical constitution and in turn lithological assemblages on the Moon provide insights into the primordial crust of the Earth–Moon system. Whereas the primordial crust was largely preserved on the Moon due to the absence of plate tectonics, the Hadean crust of Earth was destroyed and dragged down to the deep mantle soon after the plate tectonics processes (Kawai et al., 2009; Maruyama et al., 2013).

7. Conclusions

The dominant mineralogy of rock exposures in five regions of the Moon was analysed using M^3 data. The results showing pyroxenes, olivine and plagioclase corroborate with the observations in previous studies. The band shape technique offers a powerful tool in identifying minerals and also the spectrally unique pixels (end-members) can also be analysed on the image. The presence of olivine indicates komatiitic basalts, and the OH/H_2O band in the olivine suggests possible incorporation of magmatic water. The LCP occurrences in the different basins correspond to gabbroic rocks of the lower crust exposed as magmatic intrusions or exhumed during major impact. The HCP is correlated to magmatic differentiation. The plagioclase-rich domains on the Lunar surface correlates with anorthositic crust, and confirms the LMO model. The Fe-Mg-spinels might form part of mafic intrusions, or as chromite-veined anorthosites. Regular interval sampling and quantitative mineral mapping in combination with detailed crustal thickness estimates might provide further insights into the composition and evolution of the Lunar crust.

Acknowledgement

We wish to acknowledge M^3 Level-2 data team for supplying the data. We are thankful to Prof. Shaji E (Manuscript Handling Editor) and anonymous reviewers for their constructive suggestions on this manuscript.

References

Adams, J.B., 1974. Visible and near-infrared diffuse reflectance spectra of pyroxenes as applied to remote sensing of solid objects in the solar system. Journal of Geophysical Research 79, 4829–4836.

Adams, J.B., Goullaud, L.H., 1978. Plagioclase feldspars: visible and near infrared diffuse reflectance spectra as applied to remote sensing. Lunar Planetary Science Conference 9, 1–3.

Anand, M., Tartèse, R., Barnes, J.J., 2014. Understanding the origin and evolution of water in the Moon through Lunar sample studies. Philosophical Transactions of the Royal Society of London A: Mathematical. Physical and Engineering Sciences 372 (2024), 20130254.

Arivazhagan, S., 2015. Quantitative Characterization of Lunar Mare Orientale Basalts Detected by Moon Mineralogical Mapper on Chandrayaan-1. In: Planetary Exploration and Science: Recent Results and Advances. Springer, Berlin Heidelberg, pp. 21–43.

Bhattacharya, S., Chauhan, P., Rajawat, A.S., Ajai, Kumar, A.S.K., 2011. Lithological mapping of central part of Mare Moscoviense using Chandrayaan-1 Hyperspectral Imager (HySI) data. Icarus 212, 470–479.

Bhattacharya, S., Chauhan, M., Chauhan, P., 2015. Remote detection of magmatic water in association with olivine of possible mantle origin on the Moon. In: Lunar and Planetary Science Conference 46, 1396.

Borst, A.M., Foing, B.H., Davies, G.R., Van Westrenen, W., 2012. Surface mineralogy and stratigraphy of the lunarLunar South Pole-Aitken basin determined from Clementine UV/VIS and NIR data. Planetary and Space Science 68 (1), 76–85.

Burns, R.G., 1993. Mineralogical Applications of Crystal Field Theory, second ed., vol. 5. Ambridge University Press, London, England, pp. 220–242.

Cahill, J.T.S., Lucey, P.G., Wieczorek, M.A., 2009. Compositional variations of the lunar crust: results from radiative transfer modeling of central peak spectra. Journal of Geophysical Research: Planets (1991–2012) 114 (E9), 1–32.

Chauhan, P., Kaur, P., Srivastava, N., Bhattacharya, S., Kumar, A.S., Goswami, J.N., 2012. Compositional and morphological analysis of high resolution remote sensing data over central peak of Tycho crater on the Moon: implications for understanding lunar interior. Current Science 102 (7), 1041–1046.

Chauhan, P., Kaur, P., 2014. Detection of OH/H_2O on the central peak of Jackson crater from Moon mineralogical mapper (M^3) data onboard Chandrayaan-1. In: Lunar and Planetary Science Conference 45, 2072.

Cheek, L.C., Pieters, C.M., Boardman, J.W., Clark, R.N., Combe, J.P., Head, J.W., Taylor, L.A., 2011. Goldschmidt crater and the Moon's north polar region: results from the Moon Mineralogy Mapper (M^3). Journal of Geophysical Research: Planets (1991–2012) 116 (E6), 1–15.

Cheek, L.C., Donaldson Hanna, K.L., Pieters, C.M., Head, J.W., Whitten, J.L., 2013. The distribution and purity of anorthosite across the Orientale basin: new perspectives from Moon Mineralogy Mapper data. Journal of Geophysical Research: Planets 118 (9), 1805–1820.

Cheek, L.C., Pieters, C.M., 2014. Reflectance spectroscopy of plagioclase-dominated mineral mixtures: implications for characterizing lunar anorthosites remotely. American Mineralogist 99 (10), 1871–1892.
Clark, R.N., Roush, T.L., 1984. Reflectance spectroscopy: quantitative analysis techniques for remote sensing applications. Journal of Geophysical Research: Solid Earth (1978–2012) 89 (B7), 6329–6340.
Clark, R.N., King, T.V.V., Gorelick, N.S., 1987. Automatic continuum analysis of reflectance spectra. In: Proceedings, Third AIS Workshop, 2–4 June, 1987, JPL Publication 87–30. Jet Propulsion Laboratory, Pasadena, California, pp. 138–142.
Clark, R.N., 2009. Detection of adsorbed water and hydroxyl on the Moon. Science 326 (5952), 562–564.
Cloutis, E.A., Sunshine, J.M., Morris, R.V., 2004. Spectral reflectance-compositional properties of spinels and chromites: implications for planetary remote sensing and geothermometry. Meteoritics and Planetary Science 39 (4), 545–566.
Conel, J.E., Nash, D.B., 1970. Spectral reflectance and albedo of Apollo 11 lunar samples: effects of irradiation and vitrification and comparison with telescopic observations. In: Proceedings of the Apollo 11 Lunar Science Conference 3, pp. 2013–2024.
Craddock, R.A., Howard, A.D., 2000. Simulated degradation of lunar impact craters and a new method for age dating far side mare deposits. Journal of Geophysical Research: Planets (1991–2012) 105 (E8), 20387–20401.
Donaldson Hanna, K.L., Cheek, L.C., Pieters, C.M., Mustard, J.F., Greenhagen, B.T., Thomas, I.R., Bowles, N.E., 2014. Global assessment of pure crystalline plagioclase across the Moon and implications for the evolution of the primary crust. Journal of Geophysical Research: Planets 119 (7), 1516–1545.
Elrado, S.M., Shearer, C.K., Kaaden, K.E.V., McCubbin, F.M., Bell, A.S., 2015. Petrogenesis of primitive and evolved basalts in a cooling Moon: experimental constraints from the youngest known lunar magmas. Earth and Planetary Science Letters 422, 126–137.
Gillis, J., 1998. The Composition and Geologic Setting of Mare Deposits on the Far Side of the Moon (Ph.D. thesis). Rice University, Houston.
Goswami, J.N., Annadurai, M., 2009. Chandrayaan-1: India's first planetary science mission to the Moon. Lunar Planetary Science (CDROM) 40, 2571.
Haruyama, J., Ohtake, M., Matsunaga, T., Morota, T., Honda, C., Yokota, Y., Abe, M., Ogawa, Y., Miyamoto, H., Iwasaki, A., Pieters, C.M., Asada, N., Demura, H., Hirata, N., Terazono, J., Sasaki, S., Saiki, K., Yamaji, A., Torii, M., Josset, J., 2009. Long lived volcanism on the lunar far side revealed by SELENE Terrain Camera. Science 323, 905–908.
Hauri, E.H., Weinreich, T., Saal, A.E., Rutherford, M.C., Van Orman, J.A., 2011. High pre-eruptive water contents preserved in Lunar melt inclusions. Science 333 (6039), 213–215.
Hiesinger, H., Head, J.W., 2006. New views of lunar geoscience: an introduction and overview. Reviews in Mineralogy and Geochemistry 60 (1), 1–81.
Isaacson, P.J., Pieters, C.M., Besse, S., Clark, R.N., Head, J.W., Klima, R.L., Mustard, J.F., Petro, N.E., Staid, M.I., Sunshine, J.M., Taylor, L.A., Thaisen, K.G., Tompkins, S., 2011. Remote compositional analysis of lunar olivine-rich lithologies with Moon Mineralogy Mapper (M^3) spectra. Journal of Geophysical Research: Planets (1991–2012) 116. E00G11.
Jackson, C.R., Cheek, L.C., Williams, K.B., Hanna, K.D., Pieters, C.M., Parman, S.W., Salvatore, M.R., 2014. Visible-infrared spectral properties of iron-bearing aluminate spinel under lunar-like redox conditions. American Mineralogist 99 (10), 1821–1833.
Kawai, K., Tsuchiya, T., Tsuchiya, J., Maruyama, S., 2009. Lost primordial continents. Gondwana Research 16, 581–586.
Klima, R., Cahill, J., Hagerty, J., Lawrence, D., 2013. Remote detection of magmatic water in Bullialdus Crater on the Moon. Nature Geoscience 6, 737–741. http://dx.doi.org/10.1038/ngeo1909.
Kramer, G.Y., Jolli, B.L., Neal, C.R., 2008. Distinguishing high-alumina mare basalts using clementine UVVIS and lunar prospector GRS data: mare Moscoviense and mare Nectaris. Journal of Geophysical Research (Planets) 113. E01002.
Maruyama, S., Ikome, M., Genda, H., Hirose, K., Yokoyama, T., Santosh, M., 2013. The naked planet Earth: most essential pre-requisite for the origin and evolution of life. Geoscience Frontiers 4, 141–165.
Papike, J.J., Fowler, G.W., Shearer, C.K., 1997. Evolution of the lunar crust: SIMS study of plagioclase from ferroan anorthosites. Geochimica et Cosmochimica Acta 61 (11), 2343–2350.
Pathak, S., Singh, R., Chauhan, M., Bhattacharya, S., Chauhan, P., 2015. Remote observation of lunar crater Hayn for mineralogical analysis using datasets from recent lunar missions. In: European Planetary Science Congress 2015, EPSC Abstracts 10. EPSC2015–559.
Pieters, C., Boardman, J., Buratti, B., Chatterjee, A., Clark, R., Glavich, T., Green, R., Head, J., Isaacson, P., Malaret, E., et al., 2009. The Moon Mineralogy Mapper (M^3) on Chandrayaan-1. Current Science 96, 500–505.
Pieters, C.M., Boardman, J., Buratti, B., Clark, R., Combe, J.P., Green, R., Varanasi, P., 2010. Identification of a new spinel-rich lunar rock type by the Moon Mineralogy Mapper (M^3). In: Lunar and Planetary Science Conference 41, p. 1854.
Pieters, C.M., Head, J.W., Dhingra, D., Isaacson, P., Klima, R., Petro, N., Taylor, L.A., 2011. Composition of the lower crust identified at basin rings. In: EPSC-DPS Joint Meeting 1, p. 1142.
Pieters, C.M., Hanna, K.D., Cheek, L., Dhingra, D., Prissel, T., Jackson, C., Taylor, L.A., 2014. The distribution of Mg-spinel across the Moon and constraints on crustal origin. The second conference on the lunar highlands crust and new directions. American Mineralogist 99 (10), 1893–1910.
Robinson, M.S., et al., 2010. Lunar Reconnaissance orbiter Camera (LROC) instrument overview. Space Science Reviews 150, 81–124.
Sivakumar, V., Neelakantan, R., 2014. Discovery of lunar olivine with OH/H_2O band at Moscoviense basin using hyperspectral imaging spectrometer data (M^3). International Journal of Innovative Research and Review 2 (4), 119–123.
Sivakumar, V., Neelakantan, R., 2015. Mineral mapping of lunar highland region using Moon Mineralogy Mapper (M^3) hyperspectral data. Journal of the Geological Society of India 86 (5), 513–518.
Spudis, P.D., 1993. The Geology of Multi-ring Basins: The Moon and Other Planets. Cambridge University Press, New York and Cambridge, pp. 1–244.
Spudis, P.D., Reisse, R.A., Gillis, J.J., 1994. Ancient multi-ring basins on the Moon revealed by Clementine laser altimetry. Science 266, 1848–1851.
Spudis, P.D., Adkins, C.D., 1996. Morphometry o f basins on the Moon: new results from Clementine Laser Altimetry. LPS 27, 1253–1254.
Stockstill, K.R., Spudis, P.D., 1998. Geology and deposits of the Hertzsprung basin, lunar far side. In: Lunar and Planetary Science Conference 29, p. 1236.
Taylor, S.R., Bence, A.E., 1975. Evolution of the lunar highlands crust. In: Proceedings 6th Lunar Science Conference, pp. 1121–1142.
Tompkins, S., Mustard, J.F., Pieters, C.M., Forsyth, D.W., 1997. Optimisation of endmembers for spectral mixture analysis. Remote Sensing of Environment 59, 472–489.
Warren, P.H., 1985. The magma ocean concept and lunar evolution. Annual Review of Earth and Planetary Sciences 13, 201–240.
Whitten, J., Head, J.W., Staid, M., Pieters, C.M., Mustard, J., Clark, R., Taylor, L., 2011. Lunar mare deposits associated with the Orientale Impact Basin: new insights into mineralogy, history, mode of emplacement, and relation to Orientale Basin evolution from Moon Mineralogy Mapper (M^3) data from Chandrayaan-1. Journal of Geophysical Research: Planets (1991–2012) 116 (E6).
Whitten, J., Head, J.W., 2015. Lunar cryptomaria: mineralogy and composition of ancient volcanic deposits. Planetary and Space Science 106, 67–81.
Wieczorek, M.A., Neumann, G.A., Nimmo, F., Kiefer, W.S., Taylor, G.J., Melosh, H.J., et al., 2013. The crust of the Moon as seen by GRAIL. Science 339 (6120), 671–675.
Wilhelms, D.E., 1984. The geology of the terrestrial planets. In: Carr, M.H. (Ed.), National Aeronautics and Space Administration, Special Publication 469, pp. 107–205.
Wilhelms, D.E., 1987. The Geologic History of the Moon. U. S. Geological Survey Proof Paper 1348, p. 121.
Wilhelms, D.E., Howard, K.A., Wilshire, H.G., 1979. Geologic Map of the South Side of the Moon, Scale 1:5,000,000. U.S. Department of the Interior, U.S. Geological Survey, USGS Miscellaneous Investigation Series Map I–1162.
Wood, J.A., Dickey, J.S., Marvin, U.B., Powell, B.N., 1970. Proceedings of the Apollo 11. In: Lunar Science Conference, pp. 965–988.